Title: Mechanism of glycoform specificity and protection against antibody dependent enhancement by an anti-afucosylated IgG nanobody

Authors: Aaron Gupta[1]†, Kevin Kao[1]†, Rachel Yamin[1], Deena A. Oren[2], Yehuda Goldgur[3], Jonathan Du[4], Pete Lollar[5], Eric J. Sundberg[4], Jeffrey V. Ravetch[1]*

Affiliations:

[1] Laboratory of Molecular Genetics & Immunology, The Rockefeller University, New York, NY, USA.

[2] Structural Biology Resource Center, The Rockefeller University, New York, NY, USA.

[3] Structural Biology Program, Memorial Sloan Kettering Cancer Center, New York, NY, USA.

[4] Department of Biochemistry, Emory University School of Medicine, Atlanta, GA, USA.

[5] Department of Pediatrics, Emory University School of Medicine, Atlanta, GA, USA.

†These authors contributed equally to this work.

*Corresponding author. Email: ravetch@rockefeller.edu

Abstract

Immunoglobulin G (IgG) antibodies contain a single, complex *N*-glycan on each IgG heavy chain protomer embedded in the hydrophobic pocket between its Cγ2 domains. The presence of this glycan contributes to the structural organization of the Fc domain and determines its specificity for Fcγ receptors, thereby determining distinct cellular responses. On the Fc, the variable construction of this glycan structure leads to a family of highly-related, but non-equivalent glycoproteins known as glycoforms. We previously reported the development of synthetic nanobodies that distinguish IgG glycoforms without cross-reactivity to off-target glycoproteins or free glycans. Here, we present the X-ray crystal structure of one such nanobody, X0, in complex with its specific binding partner, the Fc fragment of afucosylated IgG1. Two X0 nanobodies bind a single afucosylated Fc homodimer at the upper Cγ2 domain, making both protein-protein and protein-carbohydrate contacts and overlapping the binding site for Fcγ receptors. Upon binding, the elongated CDR3 loop of X0 undergoes a conformational shift to access the buried *N*-glycan and acts as a 'glycan sensor', forming hydrogen bonds with the afucosylated IgG *N*-glycan that would otherwise be sterically hindered by the presence of a core fucose residue. Based on this structure, we designed X0 fusion constructs that disrupt pathogenic afucosylated IgG1-FcγRIIIa interactions and rescue mice in a model of dengue virus infection.

Introduction

Glycans are ubiquitous and play essential roles throughout biology. They are present in all living cells, decorating proteins, lipids, and even nucleic acids, where they help to define molecular functions. On glycoproteins, glycans often exist as structurally similar but distinct motifs, known as glycoforms. Although related protein glycoforms have an identical amino acid backbone and may differ by only a single sugar residue, they can exhibit vastly different biological functions. In this vein, some glycoforms may be markers of specific disease states or differentially contribute to protective and pathogenic mechanisms, as has been documented extensively (*1-9*). This makes precision targeting of protein glycoforms an attractive platform for clinical diagnostics and therapeutics.

Immunoglobulin G (IgG) antibodies are one such example of glycoproteins that exhibit considerable glycoform diversity. The IgG Fc domain, a homodimer, is decorated with a single complex biantennary *N*-glycan at N297 in the Cγ2 domain on each protomer, which can adopt one of thirty-six states; in combination with subclass sequence diversity, glycan heterogeneity provides hundreds of structural permutations of IgG (*10*). The core heptasaccharide of this glycan consists of two proximal N-acetyl glucosamine (GlcNAc) residues and one mannose residue connected by β-1,4 linkages, two branching mannose residues (one α-1,3, one α-1,6), and two additional terminal GlcNAc residues connected by β-1,4 linkages. This core $Man_3GlcNAc_4$ motif is present on every IgG molecule regardless of subclass and is highly conserved across species. Most importantly, it is essential for binding to Fcγ receptors (FcγRs), a family of activating and inhibitory cellular receptors for IgG that initiate a wide array of downstream protective and pathogenic effector functions, including tumor and pathogen clearance, removal

of infected or cancerous cells, modulation of lymphocyte responses, and the initiation of anti-inflammatory pathways that restrain the immune response (*11-13*).

To generate glycoform diversity, the core heptasaccharide can be extended with core fucose, bisecting GlcNAc, terminal galactose, and/or terminal sialic acid residues. Together, these secondary glycan modifications further modulate Fc-FcγR binding and contribute to the specificity of Fc-FcγR interactions, directing binding to specific FcγRs to execute critical antibody effector functions (*14-16*). The presence or absence of the core fucose, attached to the most proximal GlcNAc of the *N*-glycan, modulates the binding affinity to FcγRIIIa. IgG lacking its core fucose has 10-20-fold higher affinity for the activating FcγRIIIa due to glycan-glycan interactions between ligand and receptor (*17, 18*). Fc fucosylation is regulated during inflammation and infection, playing a role in pathogen clearance and, when dysregulated, in pathogenicity. For example, in secondary dengue infection, afucosylated IgG1 titers – and therefore the degree of FcγRIIIa engagement – correlates with and causes disease severity (*19*). In some cases of secondary dengue infection, titers of afucosylated IgG1 at the time of hospital admission predict severe disease manifestations later in the clinical course, making Fc glycan structure a valuable prognostic (*20*). Similarly, enveloped viruses such as SARS-CoV-2 and CMV induce afucosylated IgG1 that is correlated with and may predict disease outcomes (*21-23*). Similarly, studies have also shown similar phenomena in autoimmune diseases, such as neonatal alloimmune thrombocytopenia, where anti-platelet antibodies are significantly afucosylated compared to total IgG and are correlated with clinical severity (*24*). This pathway has been exploited in therapeutic antibody development with afucosylated IgG antibodies engineered for enhanced FcγRIIIa affinity resulting in augmented cellular cytotoxicity to increase the efficacy of monoclonal antibody therapeutics (*25-27*).

Unlike other glycoproteins, IgG harbors two glycans which are buried in the cleft between the two heavy chains, and are thus not solvent exposed or readily accessible on the surface of the molecule to conventional probes. We previously described an approach to overcome this challenge and successfully identified synthetic nanobodies that can distinguish fucosylated and afucosylated IgG glycoforms (*28*). These nanobodies achieved striking specificity, with no observed cross-reactivity to off-target Fc glycoforms, glycoproteins, or free glycans, constituting a novel class of biologic agents. However, the structural basis for their glycoform specificity remains unknown. In the present study, we present the crystal structures of the afucosylated IgG-specific nanobody X0 in isolation, as well as in complex with afucosylated IgG1 Fc. We describe a unique mode of recognition of afucosylated glycoforms which relies on protein-protein contacts formed by all three X0 CDRs and reveals the long and flexible CDR3 as a sensor for the buried Fc glycan. In addition, we exploited this structural information to develop X0 as a therapeutic to disrupt pathogenic afucosylated IgG1 Fc-FcγRIIIa interactions in a mouse model of antibody-dependent enhancement of dengue virus infection. These structural and functional studies characterize the mechanism of a novel class of nanobodies and provide insights into the design of additional glycoform-specific reagents that may have broad clinical impact.

Results

Crystal structure of the afucosylated IgG-specific nanobody X0.

Several structures of nanobodies derived from the synthetic camelid nanobody library used in this study have been reported in the literature (*29, 30*). However, glycoform-specific nanobodies deviate in CDR sequence from these published models, likely resulting in significantly different loop architecture and requiring that we solve the structure of our clones in isolation. We crystallized an intermediate affinity (~142 nM) afucosylated IgG-specific clone, X0, and determined its structure by molecular replacement, using its predicted structure from AlphaFold 2 as a search model (*31, 32*), to a resolution of 1.8 Å (Fig. S1A, Table 1). The loop architecture of the crystal structure for CDR1 (residues 26-34) and CDR2 (residues 46-58) aligned very closely with its predicted structure, however, electron density for CDR3 (residues 91-108) deviated considerably and packed closer to the globular Ig fold of the nanobody than predicted. Consistent with the previously mentioned characteristics of camelid nanobodies, the CDR3 loop protruded considerably from the main body of the molecule, indicating its inherent flexibility and potential to reach recessed epitopes, such as the *N*-glycans buried in the cleft of IgG molecule (*33*).

Architecture of the X0-afucosylated IgG1 Fc complex.

To define the molecular interactions between afucosylated IgG Fc-specific nanobodies and IgG1, we determined two crystal structures of X0 in complex with afucosylated IgG1 Fc (Fig. 1A). Co-crystallization of IgG1 Fc is typically difficult due to the propensity of the Fc fragment to crystallize independently of its binding partners. To overcome this potential hurdle, we generated E382X mutants (E382A, E382R, and E382S) that have recently been reported to

reduce salt-bridge interactions between E382 and R255 that are commonly seen in the $P2_12_12_1$ space group (such as PDB: 3AVE), more easily allowing for non-canonical crystal packing arrangements (*34*). The *C*2 structure was determined by molecular replacement and multiple rounds of refinement using unliganded Fc (PDB 3AVE) and our X0 structure described above as search models. The $P6_1$ structure was determined by molecular replacement using the C2 structure as a search model. In both complexes, electron density resolved all amino acids of X0, residues 237-444 of IgG1 Fc, and the core *N*-linked heptasaccharide at N297 on both Fc chains. Additionally, a lack of electron density at the position of the core fucose corroborated the afucosylation status of our IgG Fc molecules. The final structures were refined to 2.6 A□ for *C*2 and 2.7 A□ for $P6_1$ (Table 1), and were nearly identical structurally, with an RMSD of 1.5 A□.

In both crystal structures, the X0-IgG Fc complex consists of two X0 nanobodies bound to one Fc homodimer, reflecting ability of X0 to recognize both open surfaces of the symmetrical Fc domain. Because the Fc fragment was used for these structural studies, it is possible that the presence of Fab domains in a full-length afucosylated antibody would prevent secondary X0 binding. To address this, we confirmed the stoichiometry of this interaction with by analytical ultracentrifugation of X0 mixed with full-length afucosylated IgG1 (Fig. S2). This mode of IgG recognition by the X0 nanobody contrasts with that of FcγRs, which asymmetrically intercalate within the groove of the Fc homodimer, precluding binding of a second FcγR molecule and resulting in a complex consisting of one FcγR bound to one Fc homodimer.

All CDR loops of X0 interact with the protein backbone of IgG1 Fc.

Superposition of the apo and bound structures of X0 revealed minimal changes in the CDR1 and CDR2 loop position upon binding to IgG Fc. However, consistent with an induced-fit

model, the CDR3 loop undergoes a large conformational shift, curling downwards and wrapping around the IgG C'E loop to gain better access to the buried *N*-glycan at N297. This is demonstrated by several CDR3 residues that in some cases move >9 A☐ upon binding (Fig. 1C). All three CDR loops of X0 contact the Fc protein backbone (Fig. 2A). Notably, all hydrogen bonds between X0 and the Fc fragment occur within the C'E loop of the Fc, which harbors the *N*-glycan and is a region critical for FcγR binding. Within the CDR1 loop, the sidechain of Y31 forms a hydrogen bond with $O\varepsilon^2$ of E269. T33 forms hydrogen bonds with the sidechains of Y296 and S298 as well as the main chain nitrogen of S298. Y37 forms a hydrogen bond with Y296 of the Fc (Fig. 2B). In the CDR2 loop, the main chain nitrogen of W53 forms a hydrogen bond with the side chains of E294 and S298 (Fig. 2C). The main chain nitrogen of G54 hydrogen bonds with $O\varepsilon^2$ of E294. Finally, in the CDR3 loop, $O\delta^2$ of D98 hydrogen bonds with Y296, while the main chain oxygen of G100 forms a hydrogen bond with $N\delta^2$ of N297 (Fig. 2D).

X0 was generated through affinity maturation of a previously published low-affinity parental clone, C11 (*28*). During this process, some residues were conserved across all clones and we suspected these were important for high affinity X0-IgG1 Fc binding (Fig. S3). The importance of some of these residues (F47, T52, and Y58 in CDR2; Y106 in CDR3) as well as select aforementioned X0 binding residues was experimentally validated by generating single alanine mutants at the indicated positions. Similarly, we generated afucosylated alanine mutants of the putative binding residues of IgG1 Fc, as well as other residues known to be important for FcγR binding: BC loop (H268, E269), C'E loop (E294, Y296), and FG loop (L328, P329, I332). The relative positions of these putative interactions are highlighted (Fig. 2A-D), and the impact of all mutants are shown as $\log_2$ fold change in K_D relative to wildtype X0-Fc binding (Fig. 2E). All X0 mutants reduced binding to afucosylated IgG by 4- to 30-fold and binding to fucosylated

IgG1 Fc was undetectable by SPR. C'E loop mutants completely abrogated binding, demonstrating that these residues are individually critical for X0's recognition of the Fc. The importance of interactions with Y296 explain, in part, X0's unfavorable binding to afucosylated IgG3 and IgG4, which both contain Phe at position 296. This substitution likely disrupts hydrogen bonding with T33, Y37, and D98 of X0. In contrast, both BC loop and FG loop contacts were, in isolation, dispensable for binding.

X0 CDR3 functions as the sensor for afucosylated IgG Fc glycoforms.

Two residues in the X0 CDR3 loop, G100 and T101, interact with the IgG glycan (Fig. 3A). Both of these residues were conserved across all afucosylated-specific nanobody clones, regardless of affinity. G100 and T101 are positioned at the apex of the CDR3 loop in close proximity to the *N*-glycan. The main chain N atom of G100 forms a hydrogen bond with the O7 atom of the most proximal GlcNAc (+1). In addition, the $O\gamma^1$ atom of T101 forms a hydrogen bond with the O^6 atom of the same GlcNAc residue (Fig. 3B). Importantly, this is the GlcNAc residue that is variably bonded to core fucose across all IgG glycoforms. Superimposition of the X0-IgG1 Fc complex with a previously determined fucosylated IgG1 Fc structure (i.e. PDB 3AVE) revealed that a steric clash between the core fucose and T101 would result in such a complex (Fig 3C). Accordingly, the absence of a core fucose provides a key recognition pocket for X0 which is obstructed in fucosylated IgG antibodies, suggesting that this is the mechanism governing X0 nanobody glycoform specificity (Fig. 3B, C). Consistent with its conservation during affinity maturation of C11, site-saturation mutagenesis at position 101 showed reduced binding across all mutants (Fig. 3D). Mutants with residues of similar size (Ile, Ser) or ability to

form hydrogen bonds (Gln, Glu) were generally more favorable than others, but nevertheless there was a clear preference for Thr.

X0 CDR3 recapitulates the unique carbohydrate-carbohydrate interactions between FcγRIIIa and afucosylated IgG1

Numerous structures of IgG Fc-FcγR complexes have demonstrated asymmetric binding by FcγRs, which result in a more open conformation of the Fc, with one of the immunoglobulin domains of FcγR nestled into the groove at the IgG hinge-Cγ2 interface (*35-38*). Superimposition of the X0-Fc complex and an afucosylated IgG1 Fc-FcγRIIIa complex (PDB: 3SGK) revealed overlapping epitopes between X0 and FcγRIIIa, agreeing with previously published inhibition studies (*28*) (Fig. 4A). FcγRIIIa's preference for afucosylated IgG1 Fc is a result of interactions between its oligomannose glycan at N162 and the complex *N*-glycan of IgG Fc (*17, 39*). Specifically, hydrogen bonds are formed between the first two core GlcNAc residues of the receptor and the most proximal GlcNAc of the IgG Fc. Specifically, O3 of GlcNAc1 (FcγRIIIa) binds O7 of GlcNAc1 (IgG1 Fc) and O6 of GlcNAc2 (FcγRIIIa) binds O6 of GlcNAc1 (IgG1 Fc). These glycan-glycan interactions are weakened and/or non-existent when binding fucosylated species. In our X0-Fc structure, the X0 CDR3 loop occupies a nearly identical space as the FcγRIIIa-N162 glycan, recapitulating these exact interactions (Fig. 4B, C).

X0-Fc fusions prevent antibody dependent enhancement of dengue infection

Given previous data demonstrating the capacity for nanobody-mediated blockade of Fc-FcγR interactions (*28*), we explored whether clone X0, with intermediate affinity and high

specificity, could be used *in vivo* as a therapeutic. One phenomenon that implicates Fc-FcγR interactions in disease pathogenesis is antibody-dependent enhancement (ADE) of dengue virus (DENV) infection. In humans, dengue infection often manifests as mild or inapparent disease. However, 10% of patients progress to more severe forms of disease, known as dengue hemorrhagic fever (DHF) and dengue shock syndrome (DSS). In these cases of ADE, rather than contributing to antiviral immunity, pre-existing antibodies generated during primary infection facilitate viral entry and subsequent infection of host cells, leading to both increased infectivity and virulence. This occurs when anti-DENV antibodies, at sub-neutralizing titers, complex with the DENV virion and attach to the surface of FcγR-expressing leukocytes, utilizing the phagocytic FcγR pathway for entry (*40-42*). In agreement with these *in vitro* observations, a pathogenic role for antibodies in dengue has been demonstrated *in vivo* in mouse and non-human primate disease models using polyclonal IgG isolated from symptomatic dengue patients or monoclonal anti-dengue IgG (*43-48*).

One recent study from our laboratory generated a novel mouse model of ADE that is both permissive to DENV infection and recapitulates human Fc-FcγR interactions *in vivo (49)*. This study identified afucosylated IgG1-FcγRIIIa interactions as the chief determinant of ADE severity. While pre-treatment of mice with Fc null anti-DENV monoclonal antibodies (clone C10) protects against dengue infection, afucosylated IgG1 enhances disease, evident from severe weight loss, thrombocytopenia, and eventual death (Fig. 5A). We sought to disrupt this glycoform specific Fc-FcγRIIIa interaction and prevent ADE in these mice. Pre-treatment with X0-Fc rescued mice from thrombocytopenia, severe weight loss, and death compared to isotype controls (Fig. 5B-D), demonstrating that X0 is a potential therapeutic that can selectively target afucosylated IgG glycoforms and prevent ADE.

Discussion

Glycoproteins and glycopeptide antigens are attractive targets for diagnostics and therapeutics. However, approaches to target these molecules have fallen short, as antibodies against carbohydrate antigens, as well as natural carbohydrate binding proteins, like lectins, suffer from low-binding affinities and/or poor specificity (*50-52*). Previously, we generated glycoform-specific nanobodies from a synthetic yeast display library. While we attributed their specificity to the long and flexible CDR3 domain present in camelid heavy-chain variable domains (VHHs), the structural basis of glycoform recognition was not readily evident.

In the current study, we describe the mode of recognition of an afucosylated IgG1-specific nanobody, X0. This specificity relies on two key structural properties: (i) protein-protein interactions formed by all three CDR loops of the nanobody with the protein backbone of the Fc, and (ii) a 'glycan sensor' facilitated by the highly flexible CDR3. While the protein-protein interactions by the various CDR loops are necessary for preserving affinity of these molecules, the ability of these nanobodies to discriminate between afucosylated and fucosylated Fc glycoforms is driven by the CDR3 loop. This recognition is mediated by two residues at the apex of the CDR3 loop, G100 and T101. In particular, T101 makes a critical hydrogen bond with GlcNAc(+1) on the Fc glycan, which would otherwise be sterically occluded by the presence of a core fucose. Given the importance of the CDR3 in glycoform discrimination, it is possible that nanobodies targeting other glycoproteins with solvent unexposed or recessed epitopes could be isolated, as similar findings have been demonstrated with the unique ultralong CDR3 architecture of bovine monoclonal antibodies and HIV human bnAbs (*53-55*).

In contrast to the canonical type I receptors for IgG Fc, FcγRs, for which one FcγR binds asymmetrically to one Fc homodimer, our X0 nanobody binds symmetrically with two X0 molecules binding equivalent sites on each of the two Fc protomers. Furthermore, X0 nanobody binding to IgG Fc precludes FcγR binding *in vivo*, allowing for disruption of pathogenic Fc-FcγR interactions, such as those observed in ADE of dengue virus infection and potentially those driving autoimmune disease (*24, 56, 57*). While we demonstrate direct blockade as a feasible approach for eliminating pathogenic Fc-FcγR interactions, it may also be possible to use the structure of the X0-IgG1 Fc complex to rationally design nanobody-glycosidase or protease fusions, to selectively deplete specific IgG glycoforms while preserving protective host antibodies (*58*).

To date, there have been few examples of antibodies with glycoform-level specificity (*59*). Based on our structural studies, we suspect that nanobodies may have a key advantage in recognition of buried glycan structures due to their elongated CDR3 loop. In the case of IgG, the X0 CDR3 loop can insert into the hydrophobic cleft between the two Cγ2 domains of the Fc and make hybrid protein-glycan contacts which drive specificity. Future attempts to design glycoform-specific nanobodies may benefit from further elongation and diversification of CDR3 loops to access obscured glycans. In summary, this work describes a structural basis for IgG glycoform recognition and may provide key insights into the design of future molecules.

Methods

Expression and purification of IgG, IgG Fc, and X0-Fc

Recombinant antibodies were generated using the Expi293 or Expi293 FUT8$^{-/-}$ system (ThermoFisher) using previously described protocols (*60*). An equal ratio of heavy and light chain plasmids (or only nanobody-Fc) was complexed with Expifectamine in OptiMEM and transfected into Expi293 cells in culture at 3 x 10^6 cells/ml. Enhancer 1 and 2 were added 20 hours after transfection. Recombinant IgG was harvested and purified after 6 days with protein G sepharose beads (GE Healthcare), dialyzed in PBS, filter-sterilized (0.22 μm), concentrated with 100 kDa MWCO spin concentrator (Millipore), purified with Superdex 200 Increase 10/300 GL (GE Healthcare), and finally assessed by SDS–PAGE followed by SafeBlue staining (ThermoFisher). All antibody preparations had endotoxin levels were less than 0.05 EU mg^{-1}, as measured by the limulus amebocyte lysate assay.

Expression and purification of nanobody X0

Nanobodies were expressed and purified as reported previously (*28-30, 61*). Briefly, bacteria were grown in terrific broth at 37ºC overnight. The following day, a 1:100 culture was grown until an OD of 0.7-0.9 and then induced with 1 mM IPTG. After 20-24 hours of shaking at 25ºC, *E. coli* were pelleted and resuspended in SET buffer (200 mM Tris, pH 8.0, 500 mM sucrose, 0.5 mM EDTA, 1X cOmplete protease inhibitor (Sigma)) for 30 minutes at room temperature. Following equilibration, bacteria were osmotically lysed with the addition of 2x volume of deionized water rocked for 45 minutes. Prior to centrifugation at 17,000 x *g* for 20 minutes, NaCl was added to 150 mM, MgCl$_2$ to 2 mM, and imidazole to 20 mM. The

periplasmic fraction was filtered with a 0.22 um filter and incubated with 4 mL 50% Ni-NTA resin equilibrated in wash buffer (20 mM HEPES, pH 7.5, 150 mM NaCl, 40 mM imidazole) (Qiagen) per liter of initial bacterial culture. Supernatant and resin were incubated, rocking for an hour, and then pelleted at 50 x g for 1 minute. Ni-NTA resin was washed with 10 volumes of wash buffer before elution (20 mM HEPES, pH 7.5, 150 mM NaCl, 250 mM imidazole). Eluted protein was concentrated with 3 kDa MWCO filters (Amicon) before size-exclusion chromatography (GE Healthcare). Proteins were stable at 4ºC.

Preparation and crystallization of X0-IgG1$^{E382S/A/R}$ Fc complexes

For the apo-X0 structure, X0 was purified from *E. coli* as described above. X0 was concentrated to 26 mg/mL and crystallized at room temp in the presence of MIDAS*plus* HT-96 (Molecular Dimensions) using the Art Robbins Phoenix crystallization dispenser,, in sitting-drop format, 300 nL at 1:1 ratio. The precipitant solution contained 20 % v/v PPGBA 400 + 15 % v/v 1-Propanol. Crystals were submerged in 40% ethylene glycol in the precipitant solution prior to flash cooling in liquid nitrogen.

For the X0-Fc complex structure purified X0 and the specified IgG1 Fc variant were mixed at a 3:1 ratio at room temperature for 30 minutes. The complex was isolated through size exclusion chromatography, concentrated to 35 mg/mL crystallized in the same manner as the apo-X0, using SG1 HT-96 (*P*6 complex, Molecular Dimensions) or LMB HT-96 (*C*2 complex, Molecular Dimensions). The precipitant solution for *C*2 contained, 20% w/v PEG 6000, 0.1 M Sodium citrate 4.0, 0.2 M Lithium chloride. No additional cryopreservation was necessary prior to flash cooled. The precipitant solution for *P6* contained, 0.1 M Sodium HEPES 7.5 20 % w/v

PEG 8000. Crystals were submerged in 12.5% glycerol in the precipitant solution prior to flash cooling in liquid nitrogen.

In vivo dengue antibody dependent enhancement

All in vivo experiments were performed in compliance with federal laws and institutional guidelines and have been approved by the Rockefeller University Institutional Animal Care and Use Committee. Mice were bred and maintained at the Comparative Bioscience Center at the Rockefeller University. or all experiments, Ifnar1-/- FcγR-humanized mice (males and females; 4-5 weeks old) were anesthetized with 3% isoflurane and given the monoclonal anti-DENV mAb (clone C10) in addition to X0-Fc or an isotype control 8 hours prior to infection. For infection with DENV (New Guinea C strain) mice were given 3.5×10^8 GE, i.v. Following infection, mice were weighed daily and mortality was determined once bodyweight hit an 80% threshold, as determined by the Rockefeller Institutional Animal Care and Use Committee. Platelet counts were obtained on day 0 and day 3 and measured using an automated hematologic analyzer (Heska HT5).

Data collection and structure refinement

X-ray diffraction data were collected from a single crystal at NSLS-II (Brookhaven National Laboratory) on beamline FMX (X0 alone) to 1.8 Å and AMX to 2.6 Å (C2) and 2.7 Å (P6) resolution, respectively. The data were integrated and scaled with the program HKL2000[see bottom]. Initial phase estimates and electron-density maps were obtained by molecular replacement with Phaser[see bottom] in Phenix[see bottom] using an Alphafold model

[ref see below and comment] for obtaining the X0 structure and PDB entry 3AVE for the Fc along with the X0 structure to solve the complex in C2. The C2 structure was used to solve the P6 dataset. Iterative model building and structural refinement was manually performed using COOT[see bottom] and Phenix[see bottom]. The quality of the final model was good as noted in Supplementary Table ?). All molecular graphics were prepared with Chimera [see bottom]. Atomic coordinates and experimental structure factors have been deposited in the PDB under accession codes 8F8V, 8F8X and 8F8W for X0, C2 and P6 structures.

Analytical ultracentrifugation

Sedimentation velocity analytical ultracentrifugation was conducted using an An-50 Ti analytical rotor at 50,000 rpm (182,000 x g) at a nominal temperature of 20 °C in a Beckman Coulter XLI analytical ultracentrifuge using standard procedures (*62*). Afucosylated-Fc and X0 nanobody were run individually at nominal concentrations of 3 μM and 9 μM, respectively, and together at the same concentrations. The partial specific volumes of afucosylated-Fc and X0 nanobody were calculated based on amino acid composition using SEDFIT version 16.36 (https://spsrch.cit.nih.gov/). The partial specific volume of afucosylated-Fc was adjusted using estimated fractional carbohydrate composition of 0.056 and 0.622 mL/g as the glycan partial specific volume (*63*). Samples (0.4 mL) were loaded into 12 mm pathlength Epon double sector cells equipped with sapphire windows with matched buffer (137 mM NaCl, 8.06 mM sodium phosphate, 1.94 mM potassium phosphate, 2.7 mM KCl, pH 7.4) in the reference sector. The buffer density and viscosity at 20 °C were measured using an Anton Parr DM4500 densitometer and Lovis 2000M viscometer. Absorbance scans at 280 nm were initiated after reaching the target rotor speed and collected at 4.7 min intervals. Data were corrected for scan time errors

using REDATE version 1.01 (*64*). Data were analyzed using the continuous c(s) distribution model in SEDFIT and a sedimentation coefficient interval of 0 to 10 S at 0.1 S intervals (*65*). Data were fitted using sequential simplex and Marquardt-Levenberg algorithms and maximum entropy regularization with a confidence interval of 0.68. The fitted parameters were c(s), the frictional ratio (f/f_o) and the meniscus position. Sedimentation coefficients were adjusted to the standard condition of 20 °C in solvent water.
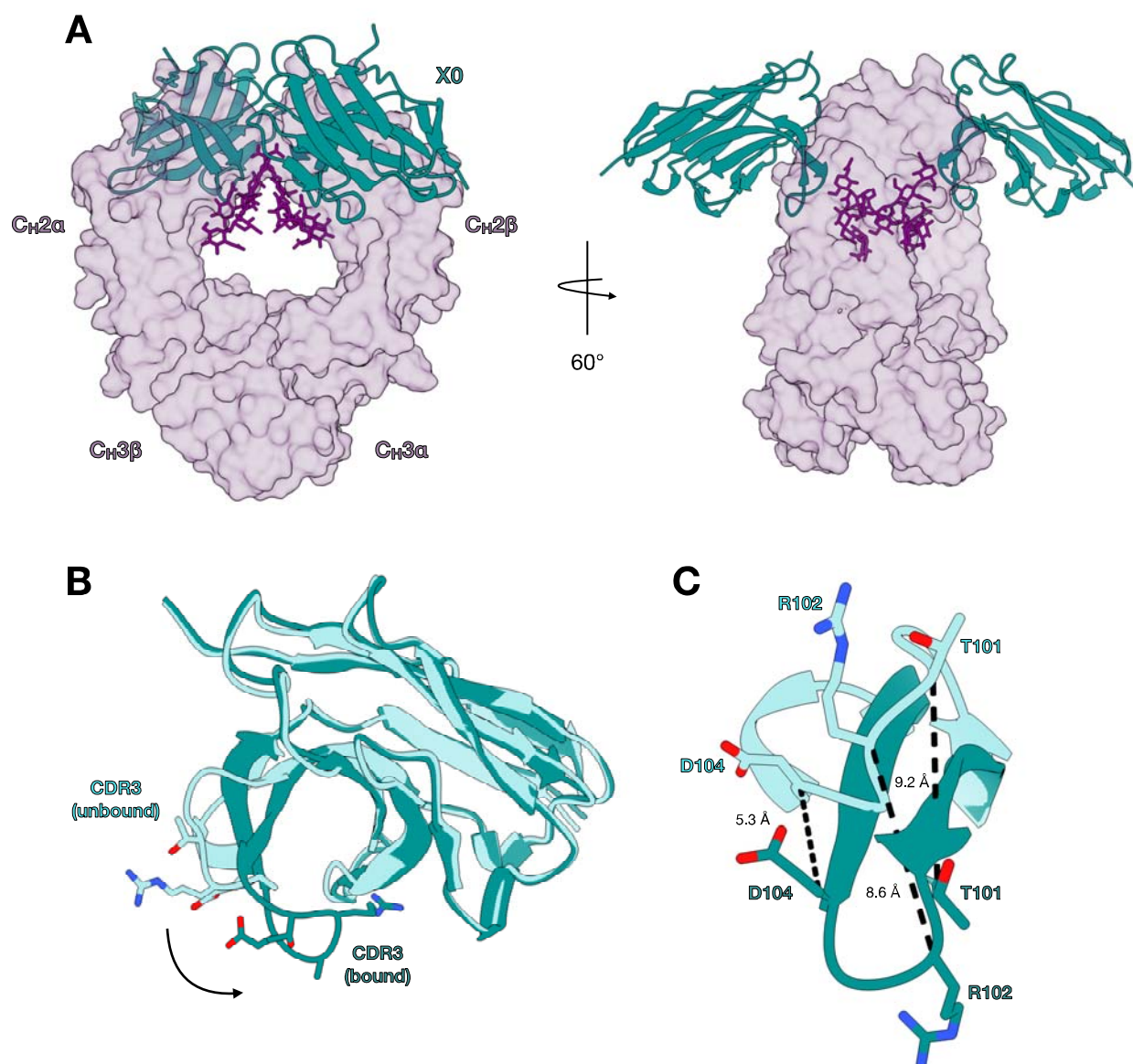
Acknowledgements

Figure 1: Overall crystal structure of the X0-afucosylated IgG1 complex. (A) Side-view (left) and top-view (right) of the complex with transparent surfaces of afucosylated IgG1 Fc (purple) and superimposed cartoons of X0 (teal) shown. *N*-glycans are shown as sticks in dark purple. (B) Unbound X0 (aquamarine) and X0 in complex (teal) superimposed, with sticks of apical CDR3 loop sidechains shown. (C) Overlay of CDR3 loops only with coloring the same as in **B**. Distances between alpha carbons of indicated sidechains shown, demonstrating an induced fit.
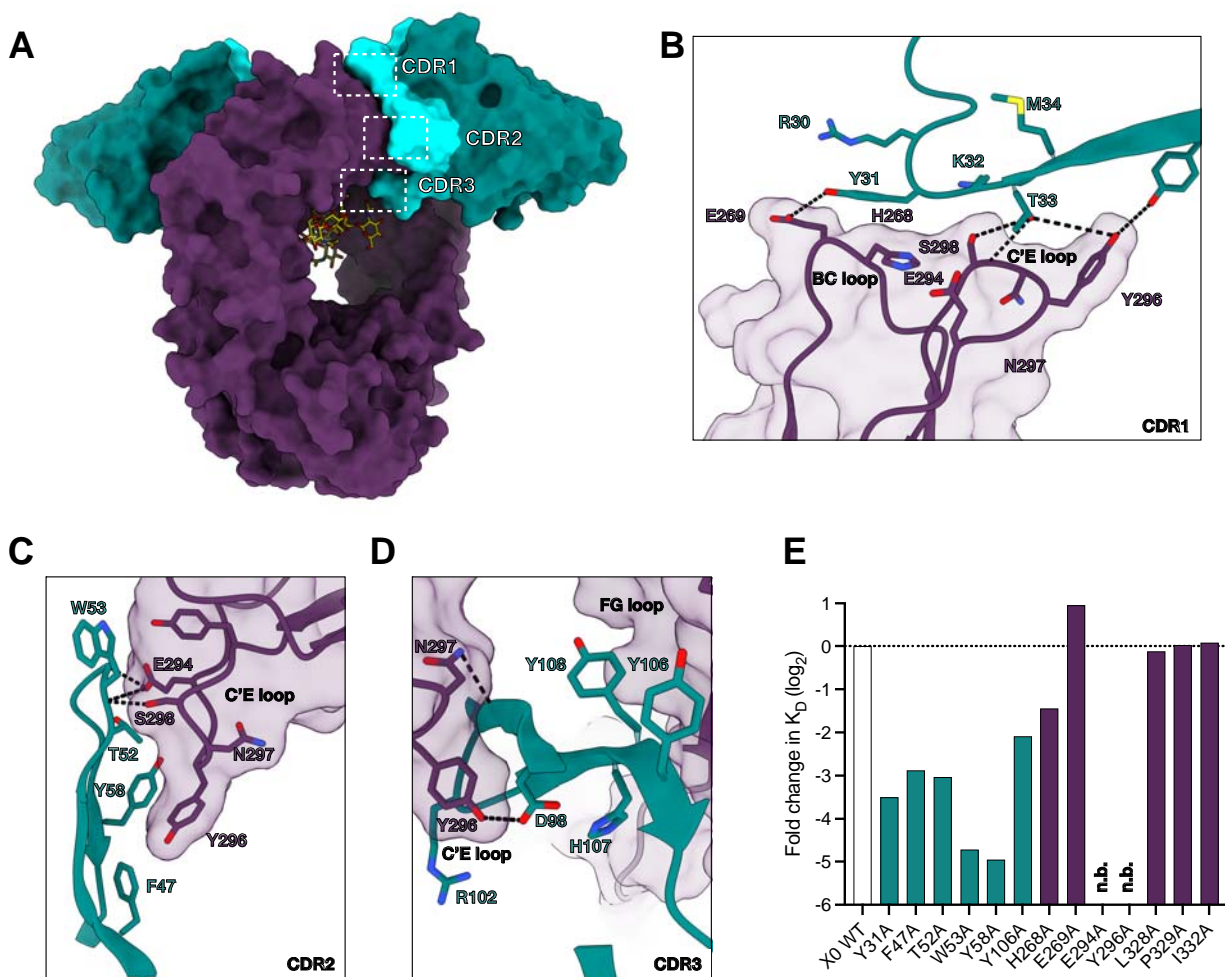
Figure 2: Protein-protein contacts at the nanobody-IgG binding interface. (A) Overall structure of the complex showing surfaces of X0 framework regions (teal), X0 CDR loops (aquamarine), afucosylated IgG1 Fc (dark purple), and stick representation of the *N*-glycans in yellow. CDR loops are highlighted by dashed white boxes. (B-D) Contact residues of CDR1, CDR2, and CDR3 with the afucosylated IgG1 Fc protein backbone. Hydrogen bonds shown as dashed black lines and bond lengths indicated. (E) Log$_2$ fold change in K$_D$ of X0 and Fc alanine mutants of putative contact sites. Horizontal dashed line represents the K$_D$ of the wildtype X0-afucosylated IgG1 Fc interaction. N.b. indicates no binding.
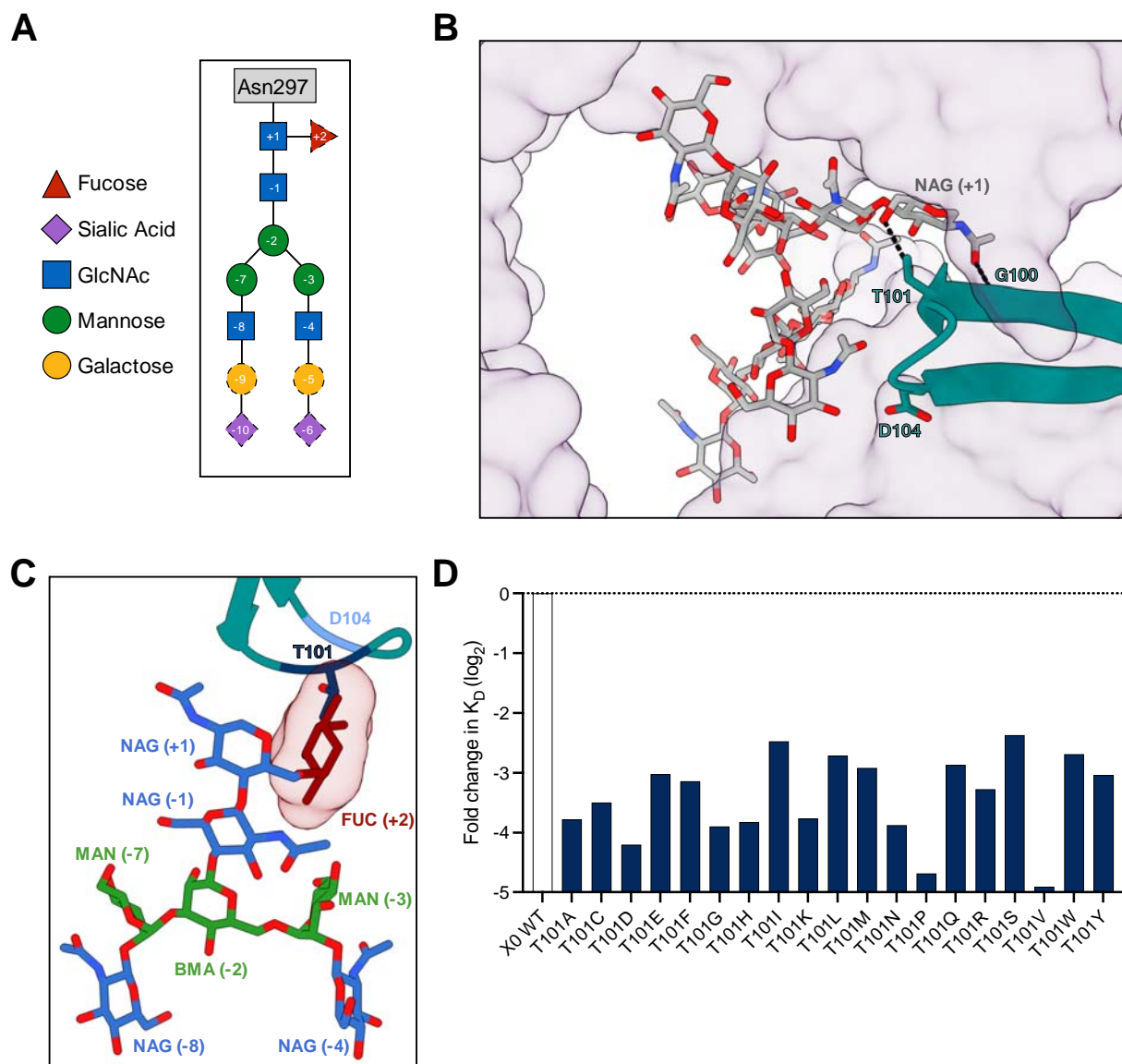
Figure 3: Protein-glycan contacts at the nanobody-IgG binding interface. (A) Schematic of the highly conserved N-glycan at IgG Fc N297. Residues colored and numbered according to SNFG standards. Residues with solid outline are part of the core $Man_3GlcNAc_4$ motif, while those with dashed outlines are variable. (B) X0 CDR3 loop contacts the Fc glycan. Hydrogen bonds shown by dashed black lines. IgG1 as transparent surface (purple), X0 as cartoon (teal), and glycan as sticks with heteroatoms shown (yellow). Relevant X0 residues highlighted in shades of blue. (C) The X0 CDR3-Fc glycan interface with the core fucose (red sticks with transparent surface) modeled in from 3AVE to reveal potential clashes. (D) Log_2 fold change in K_D of X0 T101 mutants. Horizontal dashed line represents the K_D of the wildtype X0-Fc interaction.
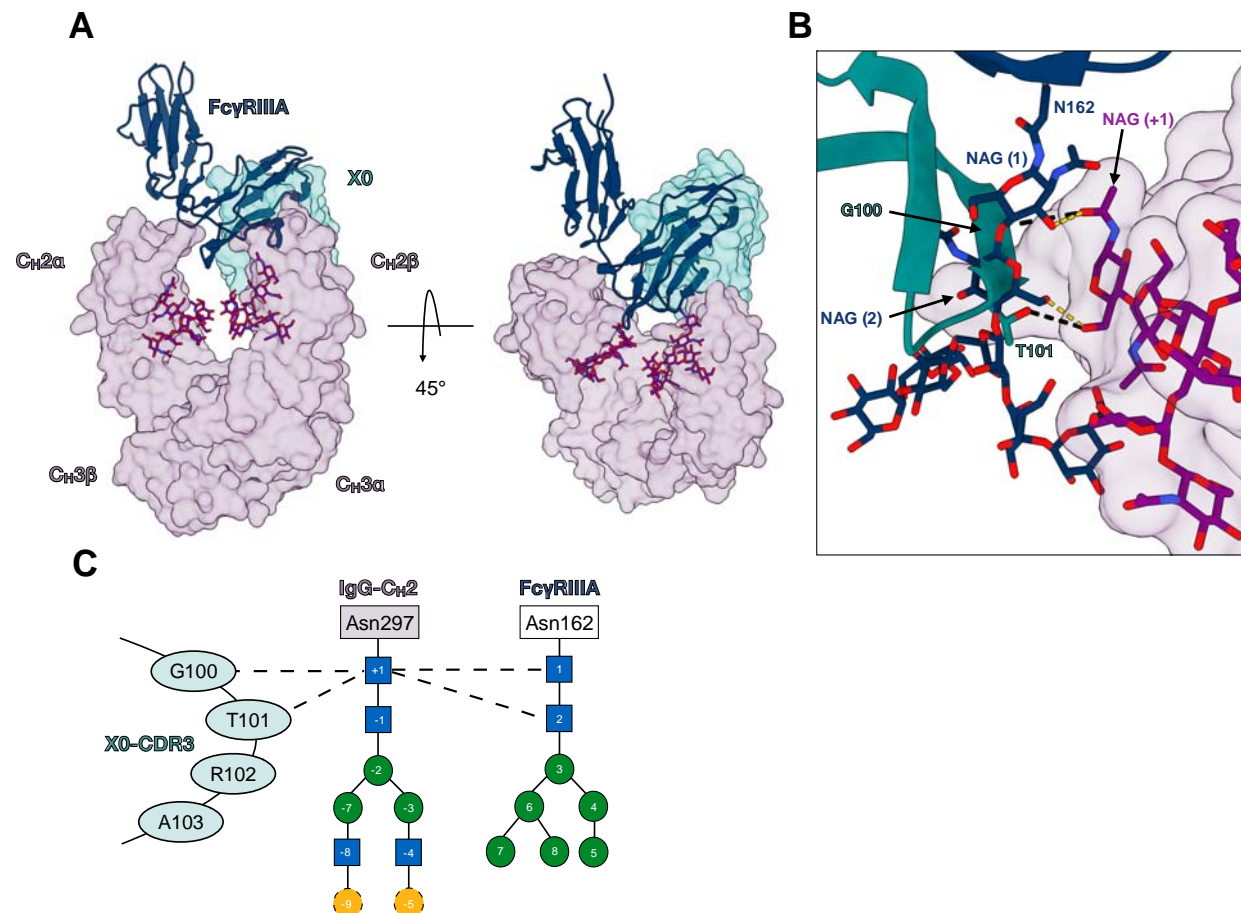
Figure 4: X0 CDR3 recapitulates the unique carbohydrate-carbohydrate interactions between FcγRIIIa and afucosylated IgG1. (A) Side-view (left) and top-view (right) of the superimposed complexes with transparent surfaces of IgG1 Fc (purple) and X0 (teal) shown as well as a cartoon of FcγRIIIa (navy). *N*-glycans are shown as sticks in purple with heteroatoms colored. (B) Close view of X0-CDR3 (teal), FcγRIIIa N162 *N*-glycan (navy sticks), and afucosylated IgG1 Fc *N*-glycan (purple surface). X0's G100 and T101 recapitulate the hydrogen bonds formed by the two proximal GlcNAcs of the FcγRIIIa N162 glycan. (C) Contact map describing X0 CDR3 and FcγRIIIa-glycan interactions with the Fc glycan. Dashed lines indicate hydrogen bonds.
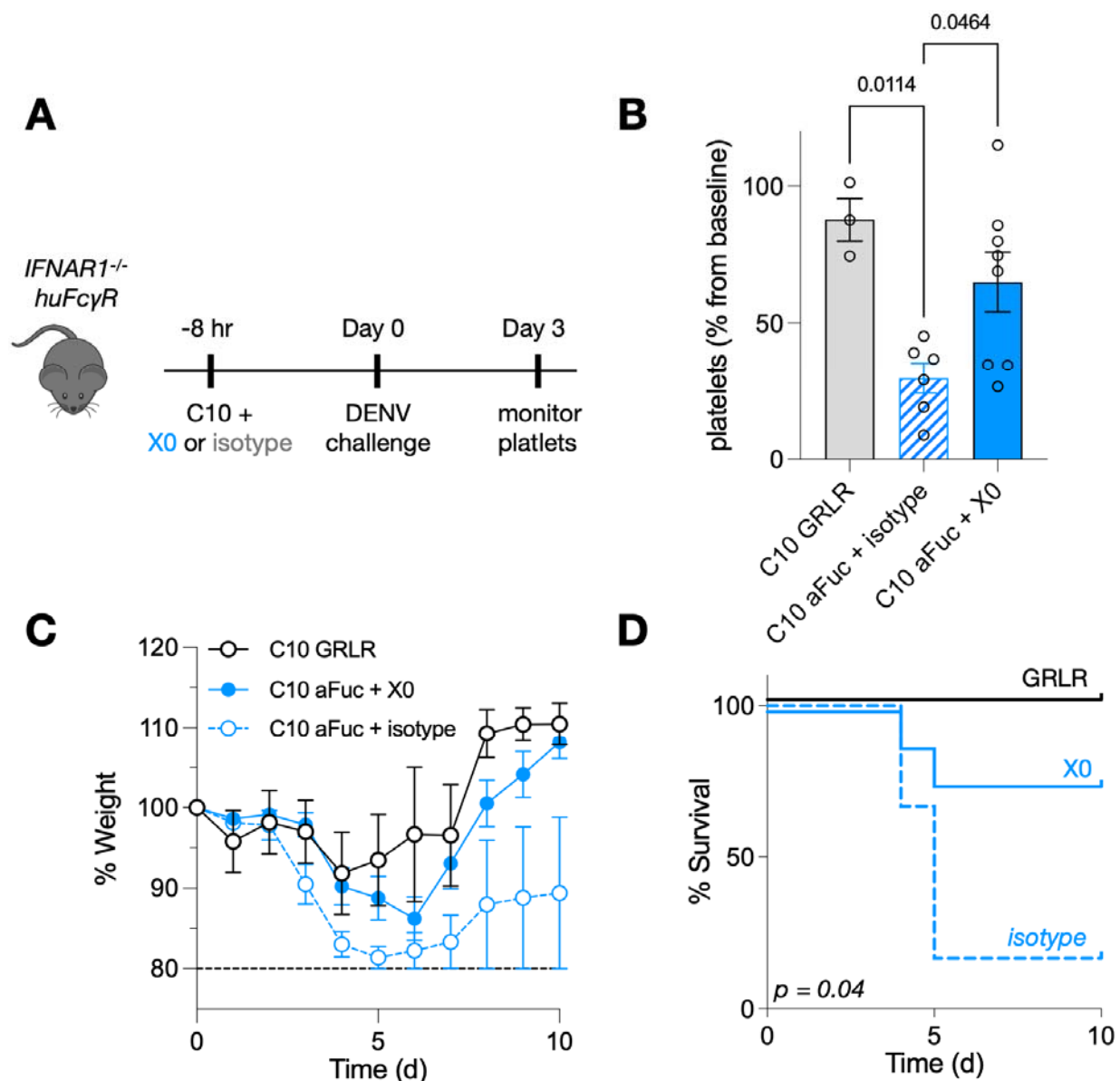
Figure 5: X0-Fc fusions block afucosylated Fc-FcγRIIa interactions to reverse antibody-dependent enhancement of dengue infection. (A) 4–6-week-old mice were administered 20 μg anti-DENV C10 along with 80 μg X0-Fc or isotype i.v., followed 8 hours later by i.v. dengue infection. Platelets were counted on days 0 and 3 and mice were monitored for weight loss and survival until day 10. (B) Platelet levels as a percentage of baseline. *P* values calculated by one-way ANOVA with Bonferroni's correction for multiple comparisons. (C) Weight as a percentage of baseline at day 0. Mice were sacrificed and excluded from further analysis if < 80% of baseline. Data displayed as mean ± SEM (n = 3-8 mice per group) in **B** and **C**. (D) Survival curves of mice treated in A. *P* value comparing X0 and isotype computed by log-rank (Mantel-Cox) test.
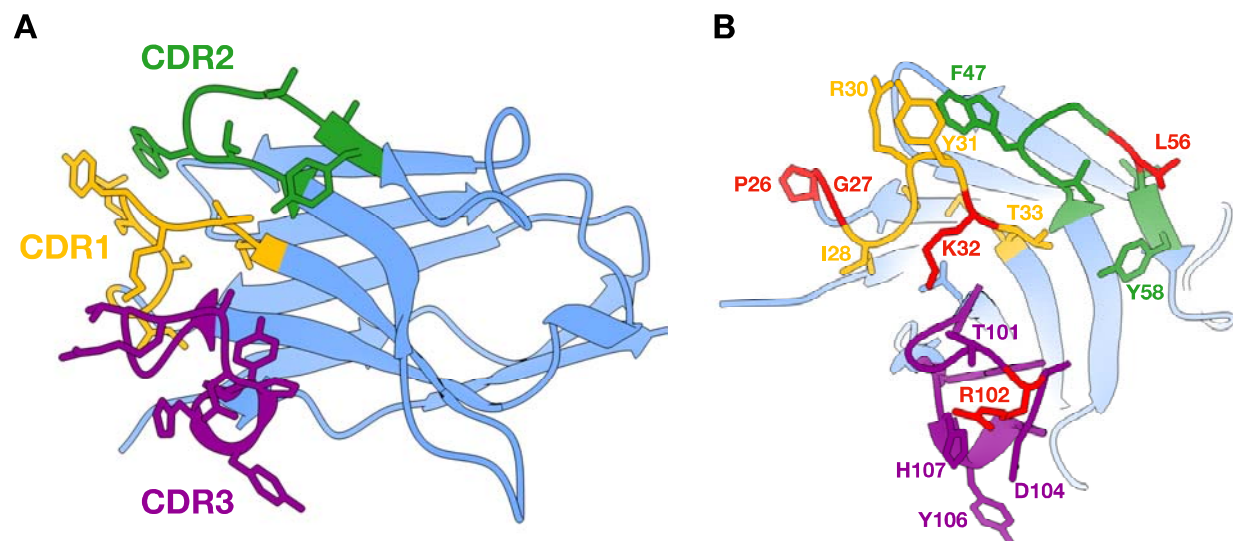
Figure S1: Crystal structure of the unbound nanobody X0. (A) Cartoon representation of the overall structure of unbound X0. Stick model of amino acid sidechains are shown for each CDR loop (CDR1 in gold; CDR2 in forest green; CDR3 in dark purple). Frame- work regions are shown in cornflower blue. (B) Straight-on view of CDR loops. Residues in red were variable during affinity maturation of C11, while those consistent with CDR coloring in **A** were conserved across all affinity-matured clones.
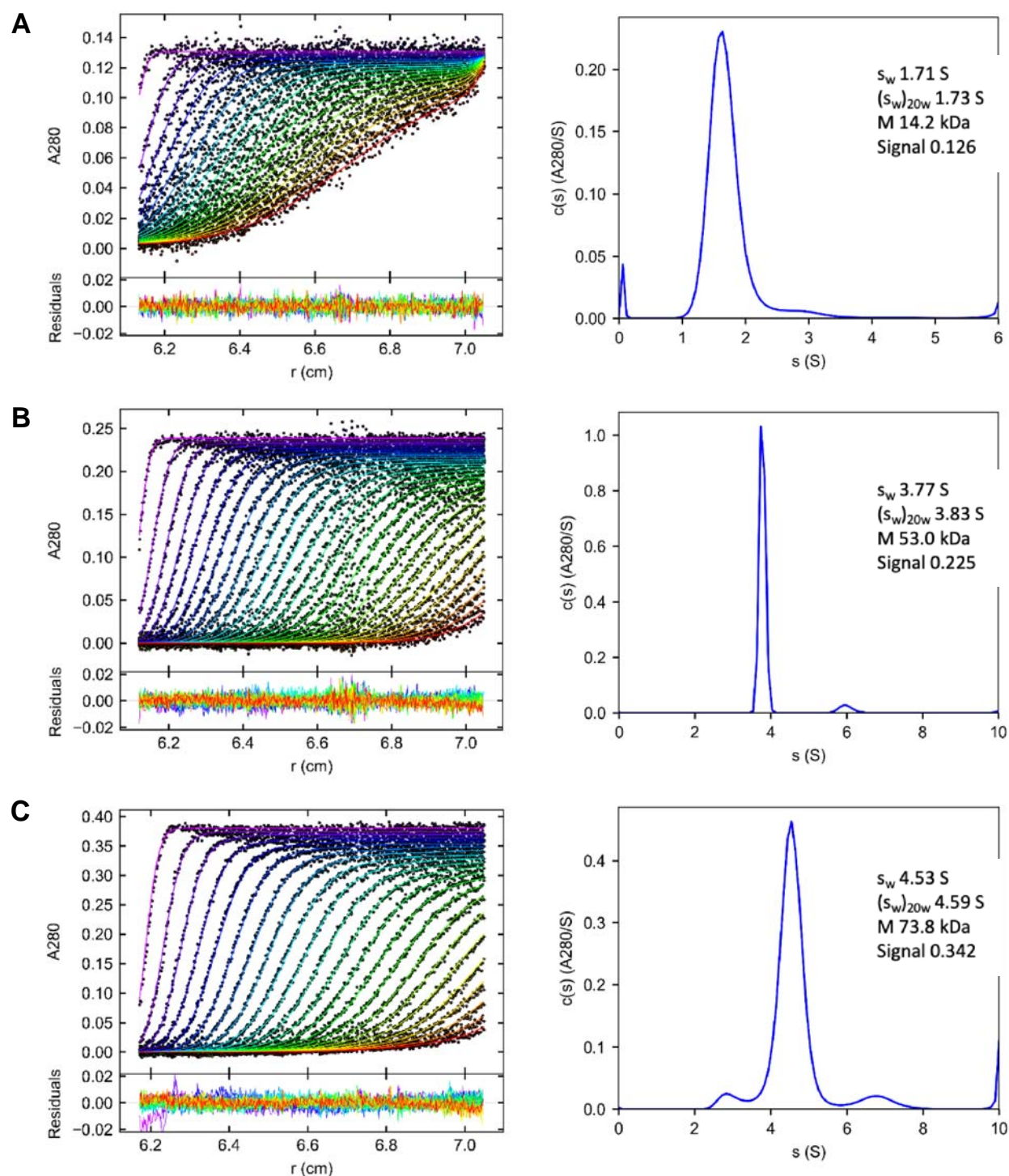
Figure S2: Analytical ultracentrifugation of the X0-IgG1 Fc complex. (A-C) Raw sedimentation profiles (left) of absorbance at 280 nm versus cell radius for X0, afucosylated IgG1 Fc, and X0-afucosylated IgG1 Fc complex and continuous sedimentation coefficient distribution (right), c(S) curve, obtained with a regularization procedure from the data.

A

Figure S3: Protein sequence alignment of afucosylated IgG-specific nanobody clones from Kao et al. (A) Clustal Omega alignment of nanobody CDR sequences and associated K_D for afucosylated IgG1. Colors indicate amino acid class (hydrophobic in orange, acidic in red, basic in blue, polar in green).

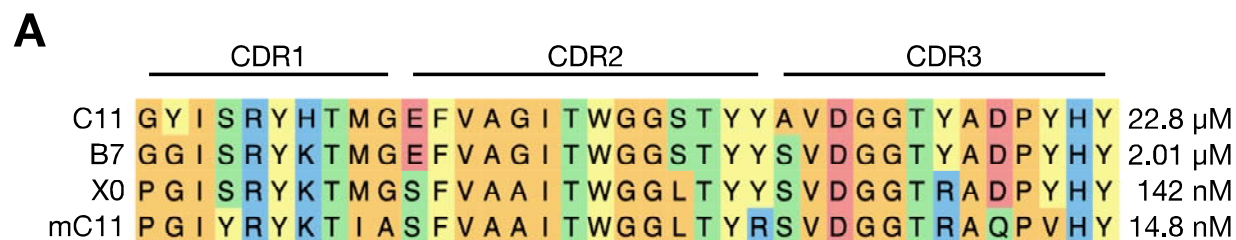|	Nanobody	Complex I	Complex II
Data collection			
Beamline	NSLS-II FMX	NSLS-II AMX	NSLS-II AMX
Space group	$I2_12_12_1$	$C2$	$P6_1$
Cell dimensions			
a, b, c (Å)	59.3, 95.1, 110.4	125.6, 92.2, 76.5	170.6, 170.6, 126.2
α, β, γ (°)	90, 90, 90	90, 117.0, 90	90, 90, 120
Resolution (Å)	50–1.8 (1.84-1.8)	50–2.6 (2.64–2.6)	50–2.7 (2.75–2.70)
Wavelength (Å)	0.97934	0.92010	0.92010
R_{pim}	0.045 (0.339)	0.050 (0.574)	0.035 (0.522)
CC(1/2)	0.991 (0.708)	0.996 (0.504)	1.000 (0.604)
$/<\sigma I>$	29.9 (1.8)	23.6 (1.4)	31.1 (1.5)
Completeness (%)	99.2 (95.8)	90.7 (90.4)	98.2 (98.9)
Redundancy	9.5 (6.7)	2.5 (2.5)	4.6 (4.8)
Unique reflections	27855	21352	56382
Phasing			
Search model	Alphafold	3AVE+nanobody	complex I
Refinement			
R_{work} / R_{free}	0.192 / 0.222 (0.289 /0.290)	0.208 / 0.279 (0.355 / 0.450)	0.220 / 0.255 (0.363/0.352)
B-factors ($Å^2$) Average/Wilson	31.2 / 23.4	78.1 / 60.2	94.0 / 71.1
RMS deviations			
bond lengths (Å)	0.007	0.015	0.012
bond angles (°)	0.959	1.95	2.06
Ramachandran plot			
% favored	98.3	96.5	97.5
% allowed	1.7	3.5	2.4
% outliers	0	0	0.1
Model contents			
Protomers / ASU	2	2	4
Protein residues	240	653	1308
Water	175	10	14
PDB ID	8F8V	8F8X	8F8W

Table 1: Data collection and refinement statistics. *Values in parentheses refer to the highest resolution shell. R_{free} set consists of 5% of data chosen randomly against which structures was not refined.*

References

1. F. Nimmerjahn, R. M. Anthony, J. V. Ravetch, *Agalactosylated IgG antibodies depend on cellular Fc receptors for in vivo activity. Proc Natl Acad Sci U S A* **104**, 8433-8437 (2007).

2. R. M. Anthony et al., *Recapitulation of IVIG anti-inflammatory activity with a recombinant IgG Fc. Science* **320**, 373-376 (2008).

3. R. M. Anthony, F. Nimmerjahn, *The role of differential IgG glycosylation in the interaction of antibodies with FcgammaRs in vivo. Curr Opin Organ Transplant,* (2010).

4. K. T. Shade et al., *A single glycan on IgE is indispensable for initiation of anaphylaxis. J Exp Med* **212**, 457-467 (2015).

5. K.-T. C. Shade et al., *Sialylation of immunoglobulin E is a determinant of allergic pathogenicity. Nature,* (2020).

6. W. Li et al., *Core fucosylation of IgG B cell receptor is required for antigen recognition and antibody production. J Immunol* **194**, 2596-2606 (2015).

7. R. G. Spiro, *Protein glycosylation: nature, distribution, enzymatic formation, and disease implications of glycopeptide bonds. Glycobiology* **12**, 43R-56R (2002).

8. M. A. Sadat et al., *Glycosylation, hypogammaglobulinemia, and resistance to viral infections. N Engl J Med* **370**, 1615-1625 (2014).

9. M. F. Jennewein et al., *Fc Glycan-Mediated Regulation of Placental Antibody Transfer. Cell* **178**, 202-215.e214 (2019).

10. M. F. Jennewein, G. Alter, *The Immunoregulatory Roles of Antibody Glycosylation. Trends Immunol* **38**, 358-372 (2017).

11. A. Pincetic et al., Type I and type II Fc receptors regulate innate and adaptive immunity. Nat Immunol **15**, 707-716 (2014).

12. S. L. Sazinsky et al., Aglycosylated immunoglobulin G1 variants productively engage activating Fc receptors. Proc Natl Acad Sci U S A **105**, 20167-20172 (2008).

13. M. J. Borrok, S. T. Jung, T. H. Kang, A. F. Monzingo, G. Georgiou, Revisiting the role of glycosylation in the structure of human IgG Fc. ACS Chem Biol **7**, 1596-1602 (2012).

14. T. Li et al., Modulating IgG effector function by Fc glycan engineering. Proc Natl Acad Sci U S A **114**, 3485-3490 (2017).

15. T. T. Wang, J. V. Ravetch, Functional diversification of IgGs through Fc glycosylation. J Clin Invest **129**, 3492-3498 (2019).

16. J. D. Pagan, M. Kitaoka, R. M. Anthony, Engineered Sialylation of Pathogenic Antibodies In Vivo Attenuates Autoimmune Disease. Cell **172**, 564-577.e513 (2018).

17. C. Ferrara et al., Unique carbohydrate-carbohydrate interactions are required for high affinity binding between FcgammaRIII and antibodies lacking core fucose. Proc Natl Acad Sci U S A **108**, 12669-12674 (2011).

18. S. Borghi et al., FcRn, but not FcγRs, drives maternal-fetal transplacental transport of human IgG antibodies. Proc Natl Acad Sci U S A **117**, 12943-12951 (2020).

19. T. T. Wang et al., IgG antibodies to dengue enhanced for FcγRIIIA binding determine disease severity. Science **355**, 395-398 (2017).

20. S. Bournazos et al., Antibody fucosylation predicts disease severity in secondary dengue infection. Science **372**, 1102-1105 (2021).

21. S. Chakraborty et al., Proinflammatory IgG Fc structures in patients with severe COVID-19. Nat Immunol, (2020).

22. *S. Chakraborty et al., Early non-neutralizing, afucosylated antibody responses are associated with COVID-19 severity. Sci Transl Med, eabm7853 (2022).*

23. *M. D. Larsen et al., Afucosylated IgG characterizes enveloped viral responses and correlates with COVID-19 severity. Science **371**, (2021).*

24. *R. Kapur et al., A prominent lack of IgG1-Fc fucosylation of platelet alloantibodies in pregnancy. Blood **123**, 471-480 (2014).*

25. *R. Marcus et al., Obinutuzumab for the First-Line Treatment of Follicular Lymphoma. N Engl J Med **377**, 1331-1344 (2017).*

26. *J. M. FitzGerald et al., Benralizumab, an anti-interleukin-5 receptor α monoclonal antibody, as add-on treatment for patients with severe, uncontrolled, eosinophilic asthma (CALIMA): a randomised, double-blind, placebo-controlled phase 3 trial. Lancet **388**, 2128-2141 (2016).*

27. *J. P. Sharman et al., Ublituximab (TG-1101), a novel glycoengineered anti-CD20 antibody, in combination with ibrutinib is safe and highly active in patients with relapsed and/or refractory chronic lymphocytic leukaemia: results of a phase 2 trial. Br J Haematol **176**, 412-420 (2017).*

28. *K. S. Kao et al., Synthetic nanobodies as tools to distinguish IgG Fc glycoforms. Proc Natl Acad Sci U S A **119**, e2212658119 (2022).*

29. *C. McMahon et al., Yeast surface display platform for rapid discovery of conformationally selective nanobodies. Nat Struct Mol Biol **25**, 289-296 (2018).*

30. *M. Schoof et al., An ultrapotent synthetic nanobody neutralizes SARS-CoV-2 by stabilizing inactive Spike. Science **370**, 1473-1479 (2020).*

31.   A. W. Senior et al., *Improved protein structure prediction using potentials from deep learning. Nature* **577**, *706-710 (2020).*

32.   J. Jumper et al., *Highly accurate protein structure prediction with AlphaFold. Nature* **596**, *583-589 (2021).*

33.   F. Gaudreault, C. R. Corbeil, E. O. Purisima, T. Sulea, *Coevolved Canonical Loops Conformations of Single-Domain Antibodies: A Tale of Three Pockets Playing Musical Chairs. Front Immunol* **13**, *884132 (2022).*

34.   A. S. Sudol, J. Butler, D. P. Ivory, I. Tews, M. Crispin, *Extensive substrate recognition by the streptococcal antibody-degrading enzymes IdeS and EndoS. Biorxiv, (2022).*

35.   Y. Sakae et al., *Conformational effects of N-glycan core fucosylation of immunoglobulin G Fc region on its interaction with Fcγ receptor IIIa. Sci Rep* **7**, *13780 (2017).*

36.   D. J. Falconer, G. P. Subedi, A. M. Marcella, A. W. Barb, *Antibody Fucosylation Lowers the FcγRIIIa/CD16a Affinity by Limiting the Conformations Sampled by the N162-Glycan. ACS Chem Biol* **13**, *2179-2189 (2018).*

37.   P. Sondermann, A. Pincetic, J. Maamary, K. Lammens, J. V. Ravetch, *General mechanism for modulating immunoglobulin effector function. Proc Natl Acad Sci U S A* **110**, *9868-9872 (2013).*

38.   P. Sondermann, R. Huber, V. Oosthuizen, U. Jacob, *The 3.2-A crystal structure of the human IgG1 Fc fragment-Fc gammaRIII complex. Nature* **406**, *267-273 (2000).*

39.   C. Ferrara, F. Stuart, P. Sondermann, P. Brunker, P. Umana, *The carbohydrate at FcgammaRIIIa Asn-162. An element required for high affinity binding to non-fucosylated IgG glycoforms. J Biol Chem* **281**, *5032-5036 (2006).*

40.   *S. B. Halstead, E. J. O'Rourke, Dengue viruses and mononuclear phagocytes. I. Infection enhancement by non-neutralizing antibody. J Exp Med **146**, 201-217 (1977).*

41.   *L. C. Katzelnick et al., Antibody-dependent enhancement of severe dengue disease in humans. Science **358**, 929-932 (2017).*

42.   *S. N. Mohsin et al., Association of FcgammaRIIa Polymorphism with Clinical Outcome of Dengue Infection: First Insight from Pakistan. Am J Trop Med Hyg **93**, 691-696 (2015).*

43.   *A. K. Pinto et al., Defining New Therapeutics Using a More Immunocompetent Mouse Model of Antibody-Enhanced Dengue Virus Infection. MBio **6**, e01316-01315 (2015).*

44.   *S. Orozco et al., Characterization of a model of lethal dengue virus 2 infection in C57BL/6 mice deficient in the alpha/beta interferon receptor. J Gen Virol **93**, 2152-2157 (2012).*

45.   *R. M. Zellweger, T. R. Prestwood, S. Shresta, Enhanced infection of liver sinusoidal endothelial cells in a mouse model of antibody-induced severe dengue disease. Cell Host Microbe **7**, 128-139 (2010).*

46.   *S. J. Balsitis et al., Lethal antibody enhancement of dengue disease in mice is prevented by Fc modification. PLoS Pathog **6**, e1000790 (2010).*

47.   *A. P. Goncalvez, R. E. Engle, M. St Claire, R. H. Purcell, C. J. Lai, Monoclonal antibody-mediated enhancement of dengue virus infection in vitro and in vivo and strategies for prevention. Proc Natl Acad Sci U S A **104**, 9422-9427 (2007).*

48.   *S. B. Halstead, In vivo enhancement of dengue virus infection in rhesus monkeys by passively transferred antibody. J Infect Dis **140**, 527-533 (1979).*

49. R. Yamin et al., Human FcγRIIIa activation on splenic macrophages drives the in vivo pathogenesis of dengue disease. Biorxiv, (2022).

50. K. Dang, W. Zhang, S. Jiang, X. Lin, A. Qian, Application of Lectin Microarrays for Biomarker Discovery. ChemistryOpen **9**, 285-300 (2020).

51. M. E. Griffin, L. C. Hsieh-Wilson, Tools for mammalian glycoscience research. Cell **185**, 2657-2677 (2022).

52. E. Sterner, N. Flanagan, J. C. Gildersleeve, Perspectives on Anti-Glycan Antibodies Gleaned from Development of a Community Resource Database. ACS Chem Biol **11**, 1773-1783 (2016).

53. D. Sok et al., Rapid elicitation of broadly neutralizing antibodies to HIV by immunization in cows. Nature **548**, 108-111 (2017).

54. Y. Zhao, S. M. Jackson, R. Aitken, The bovine antibody repertoire. Dev Comp Immunol **30**, 175-186 (2006).

55. L. Yu, Y. Guan, Immunologic Basis for Long HCDR3s in Broadly Neutralizing Antibodies Against HIV-1. Front Immunol **5**, 250 (2014).

56. R. Pfeifle et al., Regulation of autoantibody activity by the IL-23-T. Nat Immunol **18**, 104-113 (2017).

57. K. G. Smith, M. R. Clatworthy, FcgammaRIIB in autoimmunity and infection: evolutionary and therapeutic implications. Nat Rev Immunol **10**, 328-343 (2010).

58. Y. Ge et al., Target protein deglycosylation in living cells by a nanobody-fused split O-GlcNAcase. Nat Chem Biol **17**, 593-600 (2021).

59. C. L. Brooks et al., Antibody recognition of a unique tumor-specific glycopeptide antigen. Proc Natl Acad Sci U S A **107**, 10056-10061 (2010).

60.   *S. Bournazos, D. Corti, H. W. Virgin, J. V. Ravetch, Fc-optimized antibodies elicit CD8 immunity to viral respiratory infection. Nature **588**, 485-490 (2020).*

61.   *C. McMahon et al., Synthetic nanobodies as angiotensin receptor blockers. Proc Natl Acad Sci U S A **117**, 20284-20291 (2020).*

62.   *H. Zhao, C. A. Brautigam, R. Ghirlando, P. Schuck, Overview of current methods in sedimentation velocity and sedimentation equilibrium analytical ultracentrifugation. Curr Protoc Protein Sci **Chapter 20**, Unit20.12 (2013).*

63.   *J. L. Cole, J. W. Lary, T. P Moody, T. M. Laue, Analytical ultracentrifugation: sedimentation velocity and sedimentation equilibrium. Methods Cell Biol **84**, 143-179 (2008).*

64.   *H. Zhao et al., A multilaboratory comparison of calibration accuracy and the performance of external references in analytical ultracentrifugation. PLoS One **10**, e0126420 (2015).*

65.   *J. Dam, P. Schuck, Calculating sedimentation coefficient distributions by direct modeling of sedimentation velocity concentration profiles. Methods Enzymol **384**, 185-212 (2004).*